ELSEVIER

Thermochimica Acta 400 (2003) 175–185

thermochimica acta

www.elsevier.com/locate/tca

The effect of humidity on thermal process of zinc acetate

Tadashi Arii [a,*], Akira Kishi [b]

[a] *Thermal Analysis Division, Rigaku Corporation, 3-9-12 Matsubara, Akishima, Tokyo 196-8666, Japan*
[b] *X-ray Research Laboratory, Rigaku Corporation, 3-9-12 Matsubara, Akishima, Tokyo 196-8666, Japan*

Received 24 July 2002; accepted 26 September 2002

Abstract

The thermal decomposition of zinc acetate dihydrate $Zn(CH_3CO_2)_2{\cdot}2H_2O$ in some humidity-controlled atmospheres has been successfully investigated by novel thermal analyses, which are sample-controlled thermogravimetry (SCTG), thermogravimety combined with evolved gas analysis using mass spectrometry (TG–MS) and simultaneous measurement of differential scanning calorimetry and X-ray diffractometry (XRD–DSC). The thermal processes of anhydrous zinc acetate in dry gas atmosphere by conventional linear heating experiment initiated with the sublimation around 180 °C, followed by the fusion and the decomposition over 250 °C. SCTG was useful to interpret clearly the successive reaction because the high-temperature parallel decompositions were effectively inhibited. The thermal behavior changed dramatically by introducing water vapor in the atmosphere and the thermal process was quite different from that in dry gas atmosphere. Zinc oxide (ZnO) was formed only in a humidity-controlled atmosphere, and could be easily synthesized at temperatures below 300 °C. XRD–DSC equipped with a humidity generator revealed directly the crystalline change from $Zn(CH_3CO_2)_2$ to ZnO. A detailed thermal process of $Zn(CH_3CO_2)_2{\cdot}2H_2O$ and the effect of water vapor are discussed.

Keywords: $Zn(CH_3CO_2)_2{\cdot}2H_2O$; ZnO; Humidity-controlled atmosphere; Thermal process; SCTG; TG–MS; XRD–DSC

1. Introduction

Thermal decomposition of inorganic or organic crystalline salt hydrates is an important class of reactions that should be studied for a variety of potential applications to ceramic industries. For instance, low temperature synthesis via sol–gel process and/or thermal decomposition of metal-organic precursors has been widely used in various fields. Fine metal oxide powders are often synthesized by thermal decomposition of various metal-organic salts.

Zinc oxide (ZnO) is a piezoelectric material which has found wide application as illustrated by its use in acousto-electric, acousto-optic, and electro-optic devices. Recently, ZnO and related compounds have attracted much attention as one of the green fluorescent substances for the next generation of flat display. In general, such applications involve thin oxide films and past experience has shown that zinc oxide properties are significantly dependent on sample history and method of preparation. Anhydrous zinc acetate ($Zn(CH_3CO_2)_2$) has been shown to be a suitable organometallic alternative to the alkyl zinc precursors [1] for ZnO film growth by chemical vapor deposition (CVD), and is used as the source material for ZnO films grown by atomic layer epitaxy (ALE)

* Corresponding author. Fax: +81-42-544-9650.
E-mail address: t-arii@rigaku.co.jp (T. Arii).

0040-6031/03/$ – see front matter © 2002 Elsevier Science B.V. All rights reserved.
PII: S0040-6031(02)00487-2

[2]. In solution, zinc acetate has been used to deposit ZnO films by splay pyrolysis [3]. It is therefore of interest to study this zinc acetate precursor, and decomposition to form ZnO.

Several studies of the thermal decomposition of metal acetates have been reported in the literature [4–6]. Recently, the present authors investigated the thermal decomposition of metal acetate hydrate in inert atmosphere using two novel thermal analyses [7,8]: simultaneous coupling measurement of thermogravimetric–differential thermal analysis and mass spectrometry (TG–DTA–MS–MS) [9–11], and simultaneous measurement of X-ray diffractometry–differential scanning calorimetry (XRD–DSC) [12,13]. To study the underlying mechanism in detail, such complementary experimental methodologies based upon hyphenated technology, so-called three-dimensional thermal analyses, markedly improved the data interpretation.

The aim of this paper is to analyze the thermal processes of $Zn(CH_3CO_2)_2{\cdot}2H_2O$ in dry gas and some humidity-controlled atmospheres, and to investigate the affect of water vapor on the reaction mechanism and the formation temperature of ZnO. The thermal behaviors of $Zn(CH_3CO_2)_2{\cdot}2H_2O$ under such different atmospheric conditions were investigated by means of TG, sample controlled-TG(SCTG), TG–DTA–MS and XRD–DSC. The thermal path-way changed by introducing water vapor into the atmosphere and is discussed.

2. Experimental

2.1. Specimen

The powder sample of zinc acetate dihydrate ($Zn(CH_3CO_2)_2{\cdot}2H_2O$, purity 99.9%, Kanto Chemical Co. Inc.), used was the commercially available reagent without any further purification. An X-ray diffraction spectrum showed only crystalline $Zn(CH_3CO_2)_2{\cdot}2H_2O$ [14].

2.2. Apparatus

Thermogravimetric–differential thermal analysis, TG–DTA, was performed using a Rigaku Thermo Plus 8120D system equipped with SCTG mode as described in more detail elsewhere [15,16]. A sequence of experiments was carried out with a fully automated and computerized SCTG system, and the rate of mass loss was kept at an arbitrary constant value. The specimens (approximately 5 mg) were weighed into an aluminum crucible, and were heated up to 500 °C in high-purity dry helium (99.99%) and some humidity-controlled gas atmospheres, with a flow rate of 200 ml/min.

The spectra of the gaseous products evolved from the specimen in TG–DTA are simultaneously monitored with a quadrupole mass spectrometer (Q-MS; Model Thermo Mass, Rigaku). Thermo Mass system is connected to TG–DTA via a gas transfer tube with 1100 mm-long fused silica capillary of an internal diameter of 0.075 mm. Details of the TG–DTA–MS equipment are described elsewhere [17,18]. All of the transfer pathway was kept at 250 °C to minimize condensation of the gaseous products evolved from the specimen. The acceleration voltage of the ionization was fixed at potential of 70 eV. Detection mass region of m/z was fixed at 10–80. In a series of the simultaneous TG–DTA–MS experiments, to ignore desorption of any components adsorbed in the reference material such as α-Al_2O_3, only an empty platinum crucible was used as reference.

The crystal structures of the specimens quenched from TG–DTA experiments were confirmed by X-ray diffractometer (XRD; Model RINT2200V/PC, Rigaku) using graphite-monochromated Cu Kα radiation ($\lambda = 1.5405$ Å). A line shape X-ray source was operated at 50 kV and 40 mA and the data were collected in the range of $2\theta = 2$–60° with an interval of 0.02° and a scan speed of 0.5°/min.

The simultaneous measuring apparatus for XRD–DSC consisted of a specific heat-flux type of DSC (Model Thermo Plus DSC8320, Rigaku Co., Tokyo, Japan) modified and combined with an X-ray diffractometer (XRD; Model RINT-Ultima$^+$, Rigaku Co., Tokyo, Japan). Details of the XRD–DSC apparatus are described elsewhere [19]. The XRD–DSC measurements were carried out from ambient temperature to 280 °C at a heating rate of 4 °C/min. The specimen (approximately 10 mg) was mounted on a square aluminum container (7 mm × 7 mm and 0.25 mm in depth). A line shape X-ray source was operated at 50 kV and 40 mA and the data were collected in the range of $10 < 2\theta < 40^\circ$ with an interval of 0.02° and

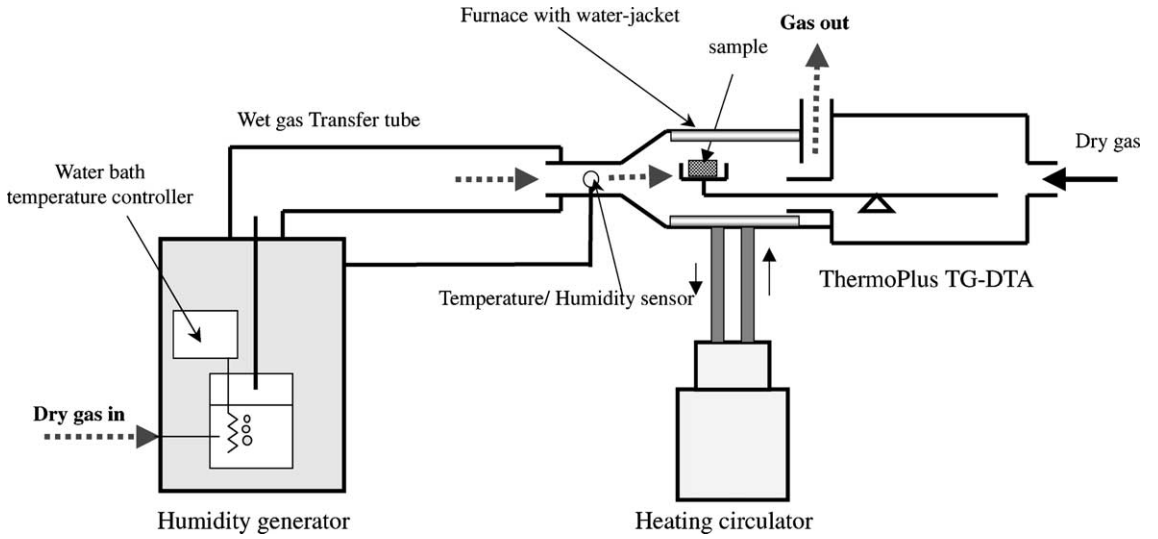

Fig. 1. Schematic diagram of integrated humidity TG–DTA system.

a scan speed of 20°/min. With a temperature scan rate of 4 °C/min, the change of sample temperature during each XRD scan corresponds to 6 °C, i.e. the XRD diagram obtained during each XRD scan expresses the mean spectrum of the temperature range of every 6 °C. The θ and 2θ calibration was done using a silicon standard.

The special type of TG–DTA equipped with an electrical furnace surrounded by a specially designed water-jacket instead of conventional type of furnace was used in order to prevent condensation of water vapor. The isothermally controlled water into the water-jacket was supplied by a heating circulator (Model F25-MV, JULABO LABORTECHNIK GMBH, Seelbach, Germany). This modified type of TG–DTA apparatus was coupled with a humidity generator (Model HUM-1, Rigaku Co., Tokyo, Japan). The schematic diagram of integrated humidity-controlled TG–DTA system is shown in Fig. 1. The mass-flow controller in the humidity generator is used to control the flow rate of dry inert gas, so that the humidity/temperature sensor located into the gas injection port of the furnace protection tube indicates constant pre-selected values. This humidity generator can provide wet gases in the humidity range from 25 °C–5%RH to 60 °C–90%RH. Additionally, the present humidity generator was also easily coupled with the XRD–DSC apparatus.

Temperature calibration of TG–DTA and DSC was performed using pure metals of In, Sn and Pb.

3. Results and discussion

3.1. Thermal process in dry gas atmosphere

The typical TG–DTA curves for $Zn(CH_3CO_2)_2 \cdot 2H_2O$ at a heating rate of 5 °C/min in dry helium flow are shown in Fig. 2. The thermal process exhibited

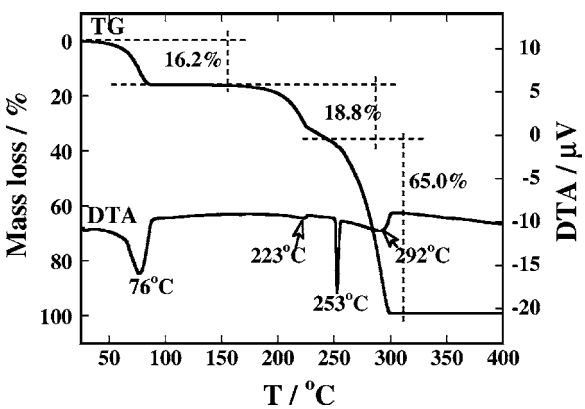

Fig. 2. Typical TG–DTA curves in helium flow for $Zn(CH_3CO_2)_2 \cdot 2H_2O$ at 5 °C/min.

several steps; no residue in the crucible was observed after the thermal analysis. The first mass loss of 16.2% up to 150 °C was accompanied by an endothermic DTA peak at 76 °C. Its mass loss agreed approximately with the theoretical value corresponding to the thermal dehydration of two water molecules (16.41%). After dehydration, the mass loss was divided into 18.8 and 65.0% by an inflection point (240 °C) resolved from the minimum between two DTG peaks. The total mass loss reaches over 99.9% at its final point (310 °C) and therefore no formation of zinc oxide was found as residue. On the other hand, the DTA curve indicated three endothermic peaks of 223, 253 and 292 °C, respectively. The first and the third DTA peaks showed the broad shapes which seem to be accompanied with the mass loss in each stage, whereas, the second DTA showed very sharp peak and appeared during the third broad DTA peak. The shape of the second DTA peak seems to be typical fusion of the specimen, but the extrapolated onset-temperature (251.2 °C) was higher than that of the reported melting point (242 °C) [20] of anhydrous zinc acetate. Fig. 3 shows a comparison of the TG–DTA curves for $Zn(CH_3CO_2)_2{\cdot}2H_2O$ at various heating rates (2, 5, 10 and 20 °C/min) in a flow of dry helium. In general, the ability to resolve TG–DTA events in conventional linear heating experiments improves with decreasing heating rate. In the present case, the mass loss observed during each stage were completely different to each other without improving the TG resolution, although the TG–DTA curves shifted to lower temperatures with decreasing the heating rate. The mass losses in the second stage especially increased with decreasing heating rate and the second mass loss reached 50.4% when heated at 2 °C/min. On the other hand, an additional sharp endothermic DTA peak appeared just before the second endothermic peak when heated above a heating rate of 10 °C/min. Both DTA peaks, at 248 and 252 °C, appeared within this temperature region. These endothermic phenomena suggested the melting processes, since both the DTA peaks were independent of the heating rates. An extrapolated onset-temperature of the former DTA peak (245 °C) was close to the melting point of anhydrous zinc acetate. Consequently, it is suggested that two different compounds were coexisted in the specimen when heated at rapid heating rate conditions. In the deposition chemistry of zinc acetate, anhydrous zinc acetate is believed to oligomerize on sublimation to form basic zinc acetate, $ZnO_4(CH_3CO_2)_6$, which is a favorable precursor for the formation of ZnO films [21]. Probably, the former DTA peak at 248 °C may be related to the formation of $ZnO_4(CH_3CO_2)_6$ and was strongly influenced by the heating rate.

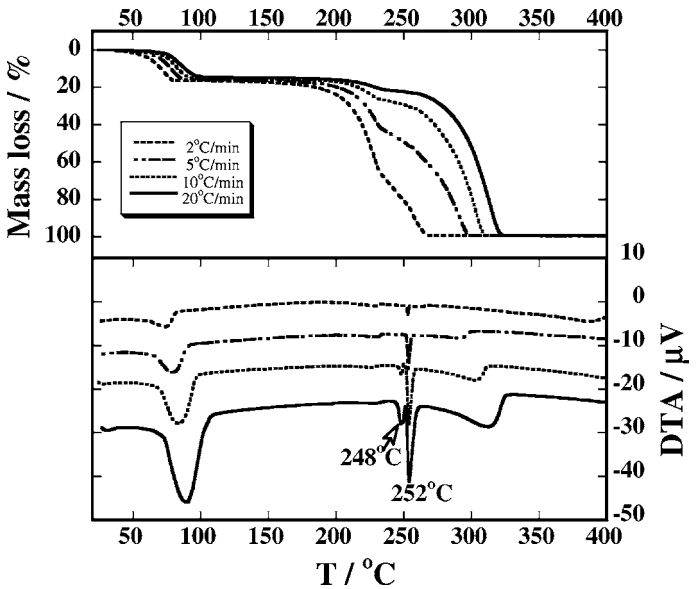

Fig. 3. Comparison of TG–DTA curves in helium flow for $Zn(CH_3CO_2)_2{\cdot}2H_2O$ under 2, 5, 10 and 20 °C/min.

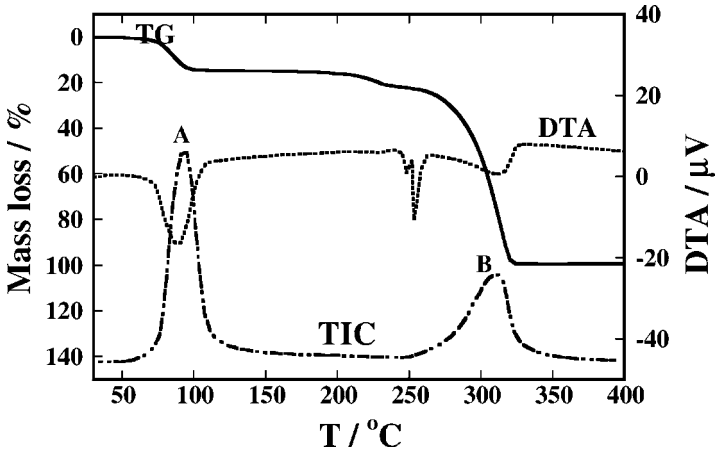

Fig. 4. Typical TG–DTA–MS results of $Zn(CH_3CO_2)_2{\cdot}2H_2O$ in helium flow at 10 °C/min.

Fig. 4 shows the typical results of TG–DTA–MS in helium flow at a heating rate of 10 °C/min, where the TIC, total ion current, indicates sum of the ion current for all detected species. Fig. 5 illustrates the mass spectra of the gases detected at the TIC peaks (100 and 310 °C), where the mass spectra indicate the signal intensities after subtracting the background spectrum before heating. The mass spectrum corresponding to the first endothermic mass loss at 100 °C proved clearly only the dehydration proceeding which was indicated by the simultaneous detection of sets of *m*/*z* 16, 17 and 18; the relative ratio of ion intensity agreed approximately with reference mass spectrum in the NIST database. On the other hand, the mass spectrum obtained from 310 °C was quite different from that of the dehydration and consisted of many ions without evolution of water vapor. By comparing with NIST database, the gases evolved were identified as a mixture of acetone (*m*/*z* 15, 28, 43 and 58) [22] and carbon dioxide (*m*/*z* 12, 28 and 44) [23] suggesting the decomposition of the specimen. The other week ions corresponded approximately to the fragmentation ions of acetone. Fig. 6 exhibits the characteristic ion intensities of *m*/*z* 18, 28, 44 and 58 as a function of the temperature, together with the TG–DTA curves. Evolution of acetone and carbon dioxide occurred concurrently during the stage, since all detected ions synchronized completely to each other. As shown in Figs. 4 and 6, no ion peaks can be observed during the second stage, although the characteristic ions in the first dehydration and the third decomposition stages are exactly corresponding to each mass loss. This fact means that not all of the gaseous components evolved during the second stage were transported to the MS ion source.

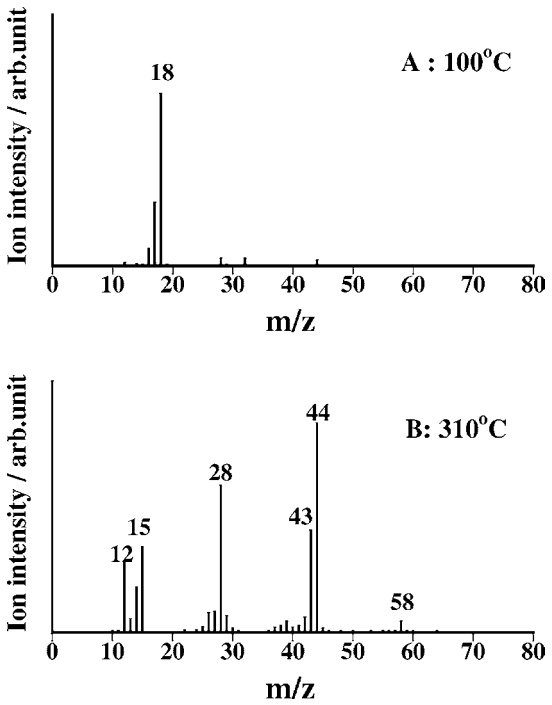

Fig. 5. Mass spectra at 100 and 310 °C.

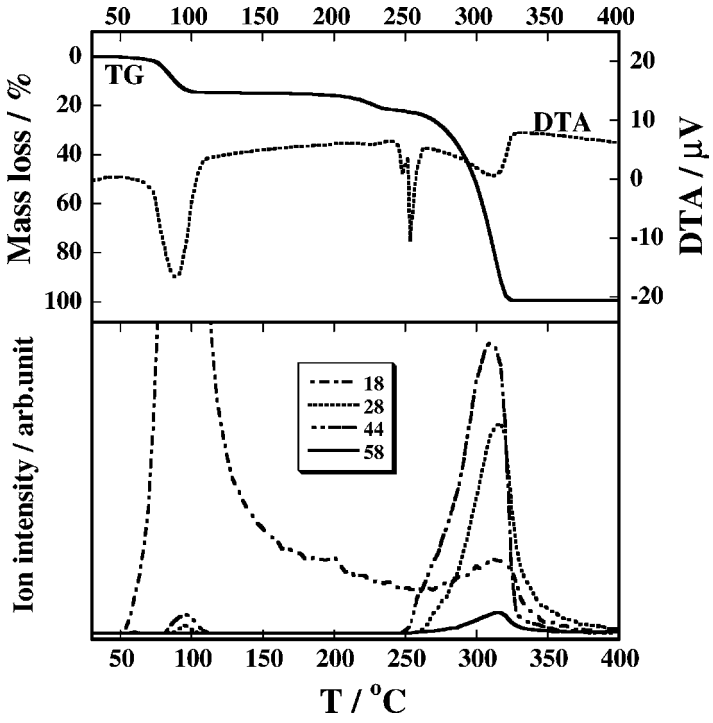

Fig. 6. Mass chromatograms of characteristic ions (*m*/*z* 18, 28, 44 and 58—*m*/*z* 18, H_2O; *m*/*z* 28, CO; *m*/*z* 44, CO_2; *m*/*z* 58, $(CH_3)_2CO$).

The typical TG–DTA–MS results of anhydrous zinc acetate at 5 °C/min by using a crucible with a pinholed lid are shown in Fig. 7. The anhydride was prepared by quenching immediately from the TG–DTA apparatus at 120 °C prior to the present thermal analysis. The TIC curve synchronized completely to the DTG curve in this case. The total mass loss of 70.1% at its final point 340 °C, was quite different from that by TG using open crucible in helium flow. We can learn that the present reaction mechanism was remarkably influenced by controlling of the escaping gases from the crucible, where the mass loss was monitored in the higher temperature side. The resulting mass loss implies that the residues in the crucible may be attributed to the compounds such as zinc oxide. The mass spectrum at the TIC peak (330 °C) was similar to that of the third TIC peak at 310 °C in Fig. 5, i.e. the evolution gases were the mixture of acetone and carbon dioxide. On the other hand, the evolved gas peak was hardly observed although the endothermic DTA peak at 252 °C appeared at exactly the same temperature as that by using the open crucible. This fact suggests that the endothermic DTA peak is attributed to the fusion process that should be independent of the mass loss.

In order to elucidate the origin of the second mass loss in Figs. 4 and 6, SCTG is useful because the high-temperature parallel reaction is inhibited by controlling the mass loss rate and resolution of the mass loss curve is generally improved. Results of SCTG are shown in Fig. 8 as function of time. The specimen was heated at a constant heating rate of 5 °C/min until a predetermined switchover temperature of 40 °C, above which the mass loss rate was kept at 0.06%/min by SCTG mode of the automatic heating/cooling control. The temperature changed dramatically as seen in the figure with pre-selected mass loss rate; only two stepwise temperature changes were clearly observed. Fig. 9 represented the SCTG curve as a function of temperature. In this figure, the TG curves of Fig. 3 are superimposed for comparison. The total mass loss value by SCTG agreed approximately with those of TG, i.e. over 99.9%. The mass loss steps were significantly different compared with the TG curves. Obviously, the thermal processes of anhydrous zinc acetate

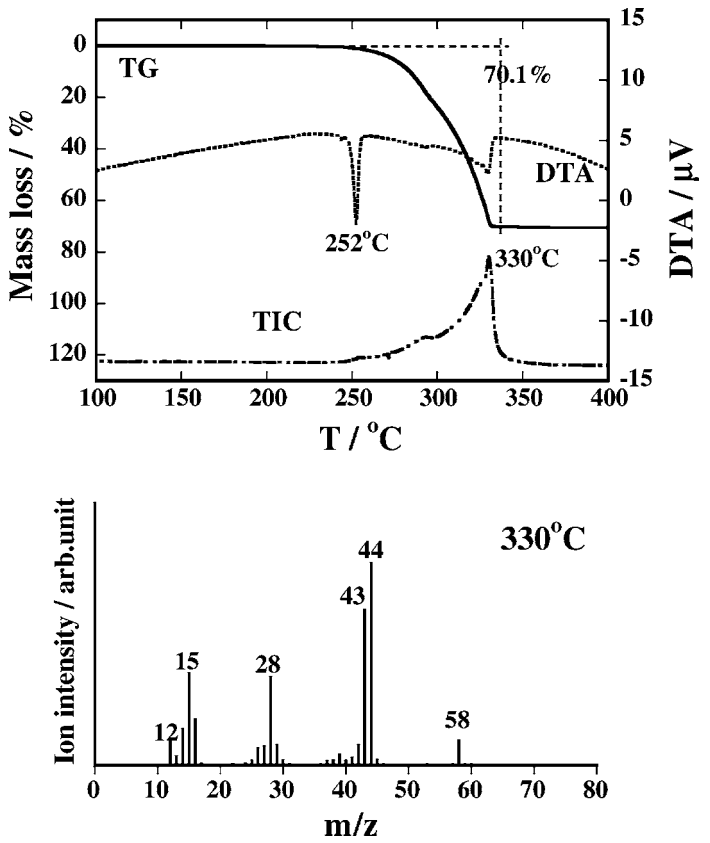

Fig. 7. Typical TG–DTA–MS results in helium flow for $Zn(CH_3CO_2)_2$ at 5 °C/min by using pinhole crucible and mass spectrum for the evolved gas at 330 °C.

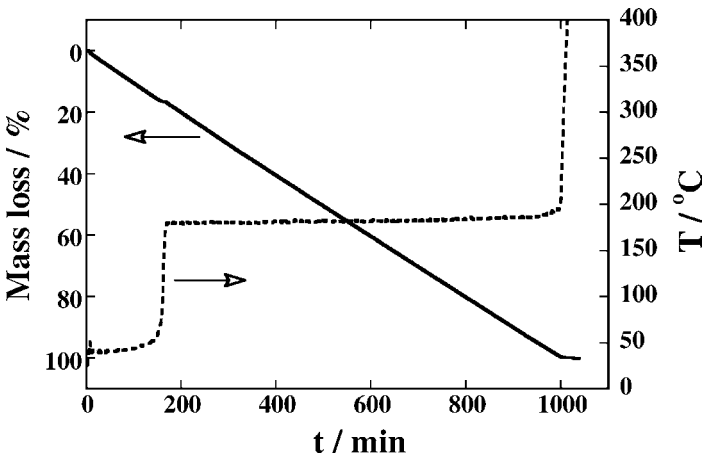

Fig. 8. Typical SCTG curve of $Zn(CH_3CO_2)_2{\cdot}2H_2O$ as function of time.

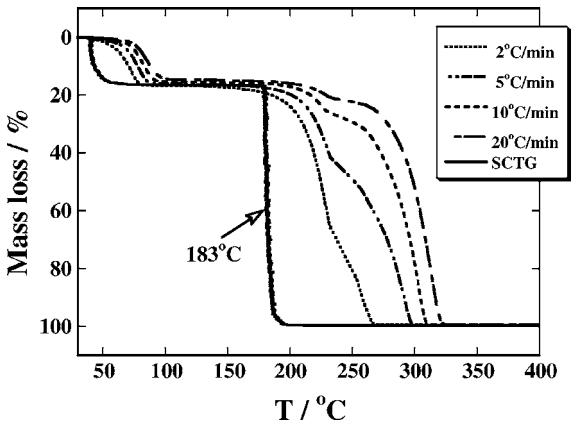

Fig. 9. Comparison of mass loss curves of $Zn(CH_3CO_2)_2{\cdot}2H_2O$ in helium flow using TG at 2, 5, 10 and 20 °C/min with SCTG at 0.06%/min.

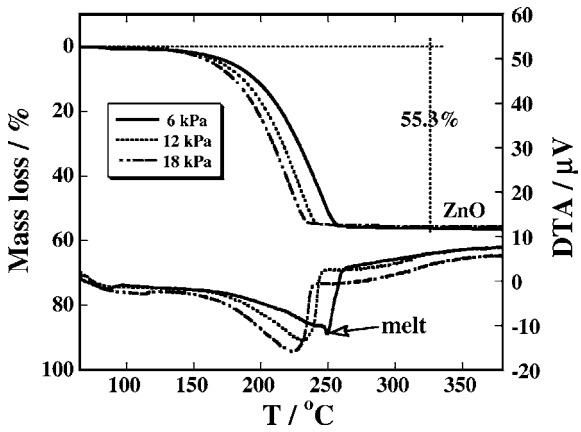

Fig. 10. Comparison of TG–DTA curves for $Zn(CH_3CO_2)_2$ at 10 °C/min under various vapor partial pressures (P_{H_2O} = 6, 12 and 18 kPa) in humidity-controlled nitrogen atmosphere.

were quite different from the TG curves; the mass loss was complete isothermally at approximately 183 °C before the fusion of the specimen. No inflectional change can be observed in course of this stage. Moreover, the shape of the SCTG curve was significantly meaningful because the mass loss of the anhydride indicated a zero-order reaction that obeys sublimation. Thus, the thermal decomposition did not occur in the present SCTG experiment. This is the reason why the mass loss values by the TG using the open crucible depended strongly upon the heating rates. It is interpreted that the sublimated gaseous component condensed immediately at the cold points in the furnace and could not reach the MS ion source. Also, these findings

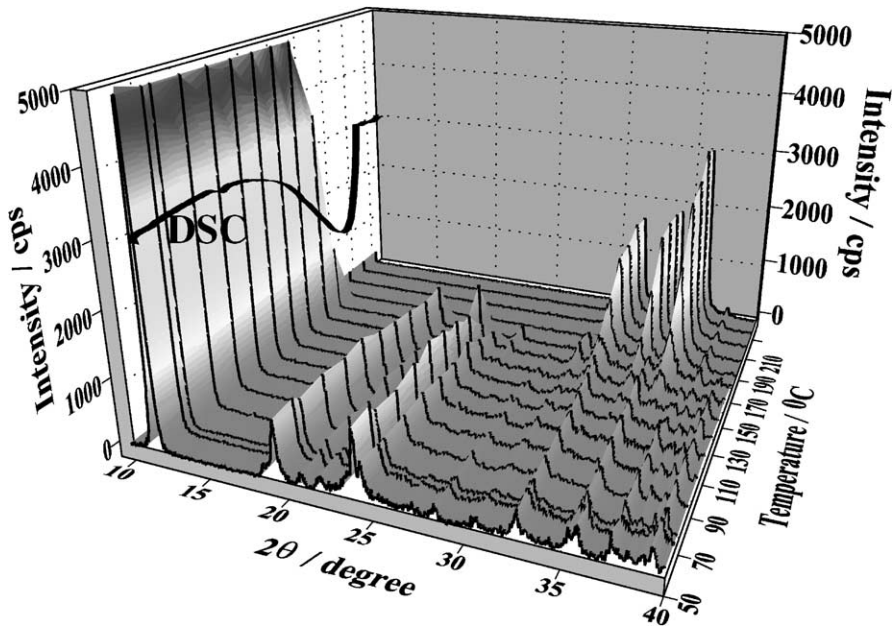

Fig. 11. Three-dimensional representation of XRD–DSC for $Zn(CH_3CO_2)_2$ at 4 °C/min in humidity-controlled nitrogen atmosphere (P_{H_2O} = 6 kPa).

suggested that the thermal decomposition of the anhydride is concurrently observed with the melting process over 250 °C when heated using relatively rapid rates.

3.2. Thermal process in humidity-controlled atmosphere

Fig. 10 illustrates a comparison of the TG–DTA curves for anhydrous zinc acetate $Zn(CH_3CO_2)_2$ at 10 °C/min under various vapor partial pressures (P_{H_2O} = 6, 12 and 18 kPa) in humidity-controlled nitrogen, where the specimens used were prepared by immediately quenching from TG–DTA at 150 °C. The thermal process was quite different from that in dry gas atmosphere. The mass loss was a simple reaction step accompanied with an endothermic DTA curve. The sharp endothermic peak showing the fusion of the specimen was found only in the humidity atmosphere using the lowest vapor partial pressure (6 kPa). It was noteworthy that the thermal processes in the humidity-controlled atmospheres were almost terminated before the melting process of anhydrous zinc acetate. The well-defined mass loss 55.3% agreed satisfactorily with the theoretical mass loss to form zinc oxide (55.3%). These findings suggest that the humidity-controlled atmosphere was capable to prevent effectively the sublimation of anhydrous zinc acetate. The similarity of the apparent TG curves is evident, except for the reaction temperatures; the TG curves shifted to lower temperature sides with increasing the vapor partial pressure. These facts are interpreted that the thermal process was remarkably influenced by the presence of water vapor and the formation of ZnO was effectively promoted with increasing the vapor partial pressure. Presumably, the formation of ZnO was speculated by allowing anhydrous zinc acetate to react with water vapor according to the reaction

$$Zn(CH_3CO_2)_2 + H_2O \rightarrow ZnO + 2CH_3COOH \quad (1)$$

where CH_3COOH represents the unidentified gaseous products.

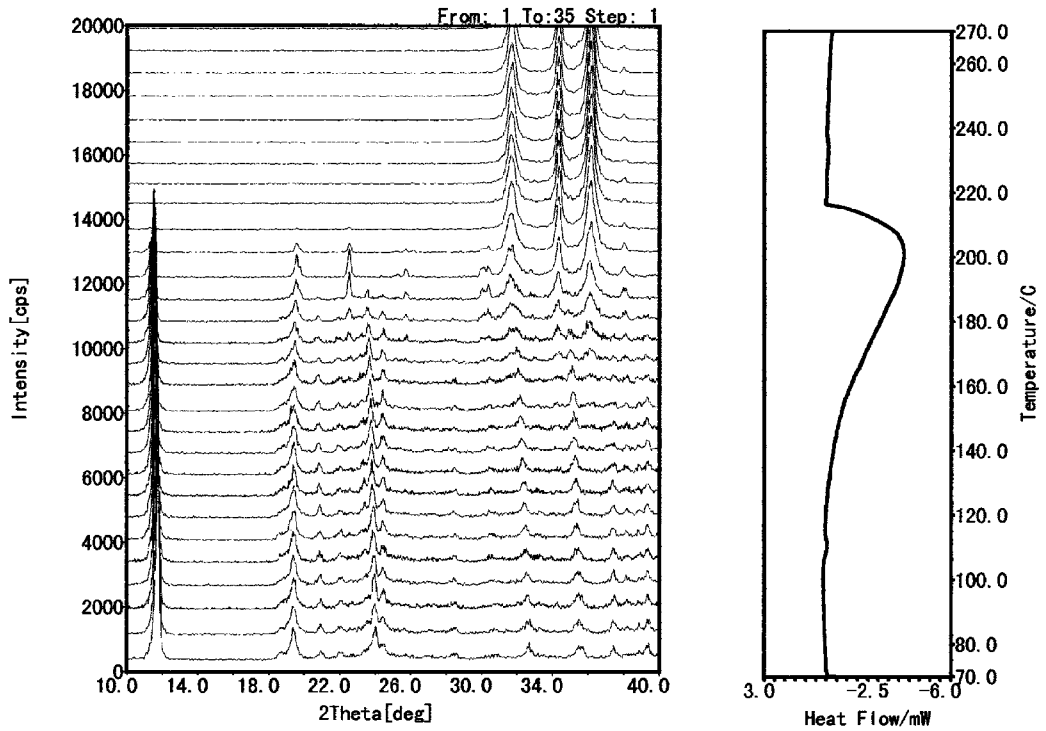

Fig. 12. Relationship between DSC curve and XRD patterns in thermal process of $Zn(CH_3CO_2)_2$ by XRD–DSC at 4 °C/min in humidity-controlled nitrogen atmosphere (P_{H_2O} = 6 kPa).

In order to prove the formation of ZnO, it is important to recognize the products formed in the solid phase. The three-dimensional representation of XRD–DSC data for anhydrous zinc acetate at 4 °C/min in a humidity-controlled nitrogen atmosphere (P_{H_2O} = 6 kPa) is shown in Fig. 11; the change of diffraction intensities in the XRD patterns clearly appeared corresponding to the DSC curve. The relationship between the XRD patterns and the DSC curve was also represented in Fig. 12; the XRD patterns corresponding to each point on DSC curve with the same temperature range are represented on the left side. The DSC curve indicates that the thermal process of the specimen begins at around 120 °C and ends at 220 °C. The shape of the DSC curve corresponds approximately with that of the DTA in Fig. 10, except for the reaction temperature. The difference should be attributed to the heating rate: 10 and 3 °C/min. The smoothness of monotonous DSC curve suggests that the present thermal process proceeded through single-step reaction without an intermediate. On the other hand, it can be clearly observed that the change in XRD patterns gradually starts from around 180 °C, and is completed after the DSC peak at 200 °C. Existence of two solid phases during the thermal process is revealed by the changing the XRD patterns. The XRD patterns obtained after the endothermic decomposition have sharp crystalline peaks, indicating pure crystalline products. The XRD profiles of the resulting products observed before and after the endothermic DSC peak agreed satisfactorily with those of anhydrous zinc acetate [24] and zinc oxide [25], respectively. The DSC curve and the integrated XRD intensity in the range of the diffraction angles characterizing the structural changes are compared in Fig. 13 as a function of temperature. The integrated intensity curve of XRD patterns of crystalline anhydrous zinc acetate shows a broad sigmoidal decay corresponding to the progress of the decomposition, while the increment of the integrated peak intensity in the diffraction angles reveals a concurrent growth of

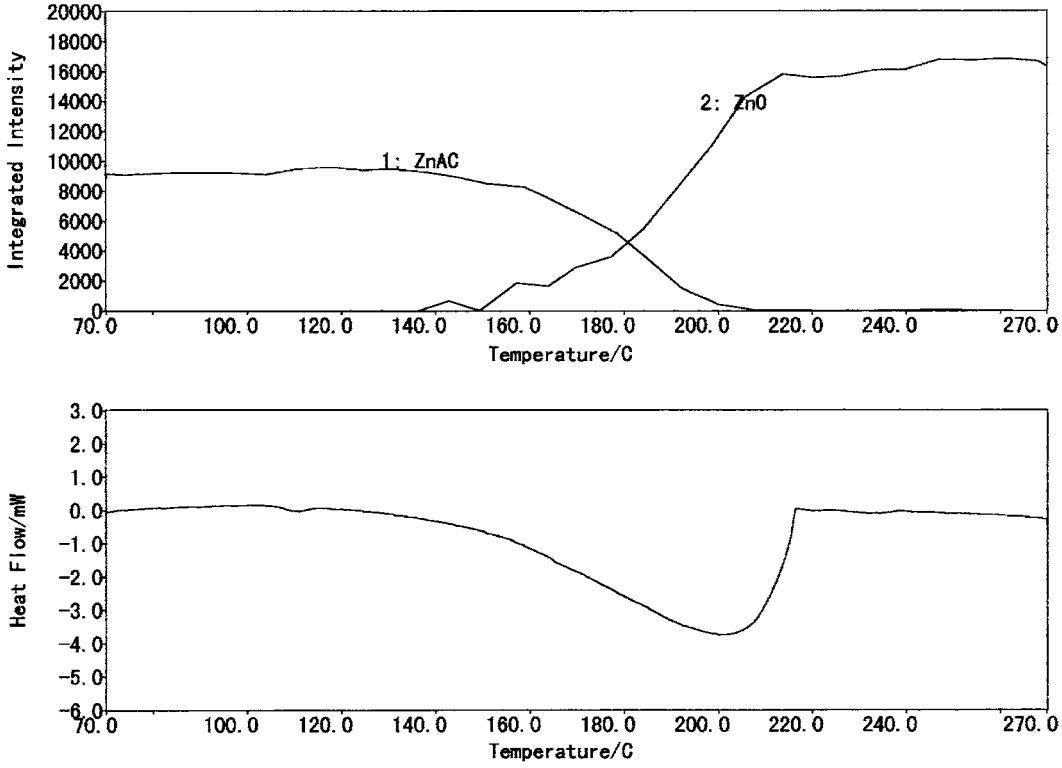

Fig. 13. Integrated intensity change of XRD peaks against temperature (upper) and DSC curve (lower) in humidity-controlled nitrogen atmosphere (P_{H_2O} = 6 kPa). Curve 1: 10–15° (zinc anhydrous acetate), curve 2: 31–38° (zinc oxide).

crystalline zinc oxide. Consequently, it is concluded that the thermal process of crystalline $Zn(CH_3CO_2)_2$ formed directly crystalline ZnO by reacting with the introduced water vapor into the atmosphere. Crystalline ZnO was easily synthesized at lower temperature region below 300 °C.

4. Conclusions

Thermal processes of $Zn(CH_3CO_2)_2{\cdot}2H_2O$ in dry and some humidity-controlled atmospheres were investigated by TG–DTA–MS, SCTG and XRD–DSC. The thermal process in dry gas atmosphere began with a single-step dehydration at ∼150 °C followed by the sublimation, fusion and decomposition, respectively. SCTG revealed that the thermal process of anhydrous zinc acetate was completed by the sublimation around 180 °C without the decomposition so that the results provided more simplified information to understand the reaction mechanism. TG–DTA–MS indicated successfully that the thermal decomposition at a higher temperature accompanied the simultaneous evolution of acetone and carbon dioxide, without the formation of zinc oxide. The thermal process of anhydrous zinc acetate is remarkably influenced by the partial pressure of water vapor in the atmosphere and was quite different from that in dry gas atmosphere. In a high humidity atmosphere, XRD–DSC revealed that anhydrous zinc acetate was directly decomposed to crystalline zinc oxide by reacting with the water vapor. Therefore, the formation of zinc oxide accelerated with increasing the partial pressure of water vapor.

These results demonstrated that novel thermal analyses such as TG–DTA–MS, SCTG and XRD–DSC are indispensable tools for determining the decomposition mechanism in sufficient detail to understand complicated thermal processes during syntheses of advanced ceramic materials. Especially, the synthesis of metal oxides via thermal decomposition of metal-organic precursors by using high humidity-controlled atmosphere will become effective in various fields as a kind of low temperature synthesis.

References

[1] A.P. Roth, D.F. Williams, J. Appl. Phys. 52 (1981) 6685.
[2] M. Tammenmaa, T. Koskinen, L. Hiltunen, M. Leskela, L. Niinesto, Thin Solid Films 124 (1985) 125.
[3] A. Ghosh, S. Basu, Mater. Chem. Phys. 27 (1991) 45.
[4] K. Manabe, M. Ogawa, Nihonkagakukaishi 7 (1983) 1092 (in Japanese).
[5] I. Mayer, F. Kassierer, J. Inorg. Nucl. Chem. 28 (1966) 2430.
[6] D.A. Edwards, R.N. Hayward, Can. J. Chem. 46 (1968) 3343.
[7] T. Arii, A. Kishi, M. Ogawa, Y. Sawada, Anal. Sci. 17 (2001) 875.
[8] T. Arii, T. Taguchi, A. Kishi, M. Ogawa, Y. Sawada, J. Euro. Ceram. Soc. 22 (2002) 2283.
[9] T. Arii, T. Senda, N. Fujii, Thermochim. Acta 267 (1995) 209.
[10] T. Arii, Y. Sawada, N. Kieda, S. Seki, J. Mass Spectrum. Soc. Jpn. 47 (1999) 354.
[11] T. Ozawa, T. Arii, A Kishi, Thermochim. Acta 352–353 (2000) 177.
[12] T. Arii, A. Kishi, Y. Kobayashi, Thermochim. Acta 325 (1999) 151.
[13] H. Yoshida, Thermochim. Acta 267 (1995) 239.
[14] Entry No. 33-1464, ICDD (zinc acetate dihydrate, $Zn(CH_3CO_2)_2{\cdot}2H_2O$).
[15] T. Arii, N. Fujii, J. Anal. Appl. Pyrol. 39 (1997) 129.
[16] T. Arii, H. Nakagawa, Y. Ichihara, N. Fujii, Thermochim. Acta 319 (1998) 139.
[17] T. Arii, Y. Masuda, Thermochim. Acta 342 (1999) 139.
[18] T. Arii, Y. Sawada, K. Iizumi, K. Kudaka, S. Seki, Thermochim. Acta 352–353 (2000) 53.
[19] A. Kishi, M. Otuka, Y. Matsuda, Coll. Surf. B: Biointerfaces 25 (2002) 281.
[20] ENCYCLOPAEDIA CHIMICA, Kyoritsu Shuppan, pp. 812–813 (in Japanese).
[21] A.K. Gyani, O.F.Z. Khan, P. O'Brien, D.S. Urch, Thin Solid Films 182 (1989) L1–L3.
[22] Entry No. 125, NIST 107 (acetone, $(CH_3)_2CO$).
[23] Entry No. 36, NIST 107 (carbon dioxide, CO_2).
[24] Entry No. 01-0089, ICDD (zinc acetate, $Zn(CH_3CO_2)_2$).
[25] Entry No. 36-1451, ICDD (zinc oxide, ZnO).